Facile Assembly of C–N Bond-Containing Polymer Electrolytes Enabled by Lithium Salt-Catalyzed Aza-Michael Addition

Jirong Wang, Chi Zhang, Yong Zhang, Gong Chen, Rinaldo Poli, Xiaolin Xie, Zhigang Xue

Facile Assembly of C-N Bond-Containing Polymer Electrolytes Enabled by Lithium Salt-Catalyzed Aza-Michael Addition

Jirong Wang,[†,#] Chi Zhang,[†,#] Yong Zhang,[†] Gong Chen,[†] Rinaldo Poli,[‡] Xiaolin Xie[†] and Zhigang Xue*[,†]

[†]Key Laboratory for Material Chemistry of Energy Conversion and Storage, Ministry of Education, Hubei Key Laboratory of Material Chemistry and Service Failure, School of Chemistry and Chemical Engineering, Huazhong University of Science and Technology, Wuhan 430074, China.

[‡]CNRS, LCC (Laboratoire de Chimie de Coordination), UPS, INPT, Université de Toulouse, 205 route de Nar-bonne, F-31077 Toulouse, Cedex 4, France

[#]Jirong Wang and Chi Zhang contributed equally.

KEYWORDS: polymer electrolyte, aza-Michael addition, lithium metal batteries, lithium salt

For Table of Contents Use Only

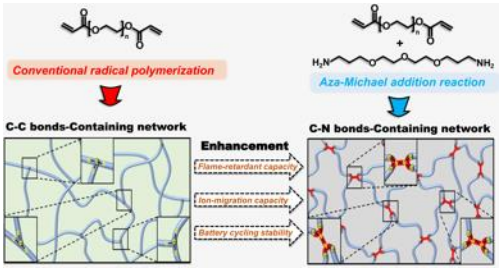

ABSTRACT: Assembling polymer electrolytes (PEs) with lithium metal anodes is a promising strategy to address safety and specific capacity concerns. Molecular design on conductive polymer matrices avoids inherent high crystallinity, poor ion transport and combustion drawbacks by adjusting the chain structure and functional groups. However, conventional structural modulation methods are difficult to be conducted via *in-situ* polymerization and cell assembly, thus hampering the further performance-enhancement of PEs in lithium batteries. Herein, we report a simple aza-Michael addition method induced by lithium salts for designing and fabricating high-performance PEs. This method fulfils the *in-situ* structure modulation of polyether-based PEs without any introduction of non-electrolytic components. The obtained polyether electrolytes exhibit a more amorphous crosslinked structure, leading to a favorable medium for ion migration and excellent flexibility. In addition, the introduction of C-N bonds imparts excellent non-flammability to the material, as well as the ability to interact with sulfolane. Hence, the *in-situ* constructed gel polymer electrolyte (GPE) is characterized by high ionic conductivity (1.76×10^{-4} S cm^{-1} at 30 ºC) and excellent interface stability with the electrodes. The assembled Li/$LiFePO_4$ (LFP) battery based on this newly designed GPE exhibits a high initial specific discharge capacity and a good rate performance (112.7 mAh g^{-1} at 5 C). Long-term stability was also demonstrated, with a capacity retention of 86.8% after 500 cycles at 1C.

INTRODUCTION

Lithium metal batteries (LMBs) have great potential for providing high energy density and long lifespan to numerous energy-storage devices.[1-4] Solid electrolytes, especially polymer electrolytes (PEs), have been identified as promising candidates to escape from the safety hazards and highly active interface reaction caused by conventional liquid electrolytes.[5-8]

However, the most used polyether-based electrolyte system is limited by the upper cut-off voltage and slack Li^+ migration due to its high crystallinity, [9, 10] tight lithium ion (Li^+) affinity[11-13] and poor interface characteristics,[7, 14] thus hampering its practical application in powering consumer electronics. In addition to the segment mobility and stability, bulk polyether is easy ignitable, and the conventional flame-retardant strategy through addition of small-molecule flame retardants yields poor compatibility with the electrodes, deteriorating the battery performance.[15-17] Inserting multiple functional groups in, or modulating the structure of the polymer matrix is an effective strategy to attenuate some inherent limitations of the polyether chains.[18, 19] However, the poor ion-conduction ability of the solid polymer electrolytes and interfacial issues with the electrodes still require the help of liquid components and *in-situ* polymerization methods.[2, 7, 20]

Gel polymer electrolytes (GPEs) prepared through *in-situ* polymerization methods can circumvent the issues of low ionic conductivity, poor electrolyte-electrode infiltration and contact, and high interfacial impedance.[5, 21-23] More importantly, the liquid phase can be carefully chosen and designed according to the structure and components of the polymer skeleton. For instance, the use of deep eutectic solvent (DES) as the plasticizer can simultaneously improve the ionic conductivity and nonflammability of the polymer electrolyte,[24-27] and its unique advantages of low-cost, simple preparation and flexible designability provide great possibility for enhancing the performance of GPEs.[28-30] Moreover, unwanted parasitic electrochemical reactions between the liquid plasticizer and the electrode are eliminated via the deliberate installation of intermolecular interactions between the polymer segments and polar liquid molecules. However, the precise GPE structural design relying on *in-situ* polymerization is unrealistic because of the difficult-to-modulate polymerization process in an enclosed battery. In addition, the conventional

initiations used in *in-situ* LMBs polymerizations are often stimulus-responsive (heating, irradiation, *etc.*), and the introduction of side reactions and non-electrolytic components may exert an adverse influence on the battery performance.[31-33] Hence, designing an efficient structure-modulation strategy for *in-situ* fabrication of gel polymer electrolytes is significantly necessary for high-performance LMBs.

The Michael addition is one of the most attractive click reactions due to its atom economy, mild reaction conditions and available raw materials, all of which conform to the principles of green chemistry.[34, 35] The main participants include a proton-bearing nucleophilic groups such as a thiol, an alcohol, or an amine, and an electrophilic alkene. Thereinto, the inherent basicity of amines triggers the addition process without the need of a catalyst,[35-37] which makes this reaction possible for the *in-situ* construction of crosslinked polymer electrolytes via utilizing bis(primary amine) and crosslinking monomer. Moreover, the reaction rate can be easily regulated by lithium salt,[38-40] which is the inherent component of electrolyte. Meanwhile, the properties of the crosslinked matrix can be modulated by the variety of diamine and the diamine/diacrylate molar ratio,[41-43] forming *in-situ* a favorable electrolyte network for ion-conduction. In addition, this reaction introduces a large fraction of C-N bonds into the polymer chains, which endows the corresponding electrolyte with unique physical and flame-retardant properties and provides abundant coordination points to interact with the plasticizer.[24, 44]

Here, we introduce a structural modulation of *in-situ* polyether-based electrolytes via a simple and mild double aza-Michael addition reaction (**Figure 1**). In comparison with crosslinked polymer (PPEGDA) formed via the conventional radical-initiated polymerization of a PEO-based diacrylate monomer (PEGDA), the aza-Michael process is more favorable without any introduction of non-electrolytic components and side reactions, and the obtained polymer

network with the introduction of abundant C-N bonds is more amorphous and nonflammable. In addition, the polar groups (C-N and C=O) in this polymer skeleton can interact with DES to fabricate an advanced GPE with good ionic conduction ability, a wide electrochemical window (5.5 V *vs* Li/Li^+, 60 °C) and stable interfacial characteristics. As a result, the assembled Li/LFP batteries exhibit obviously improved rate performance and cycling stability with respect to the pure polyether and DES systems, and the optimized lithium symmetric cell based on this GPE can steadily work at higher current density (0.5 mA cm^{-2}) without obvious dendrite-growth. The present contribution provides a simple and novel avenue for the *in-situ* regulation of the electrolyte structure and electrochemical performance of advanced and safe LMBs.

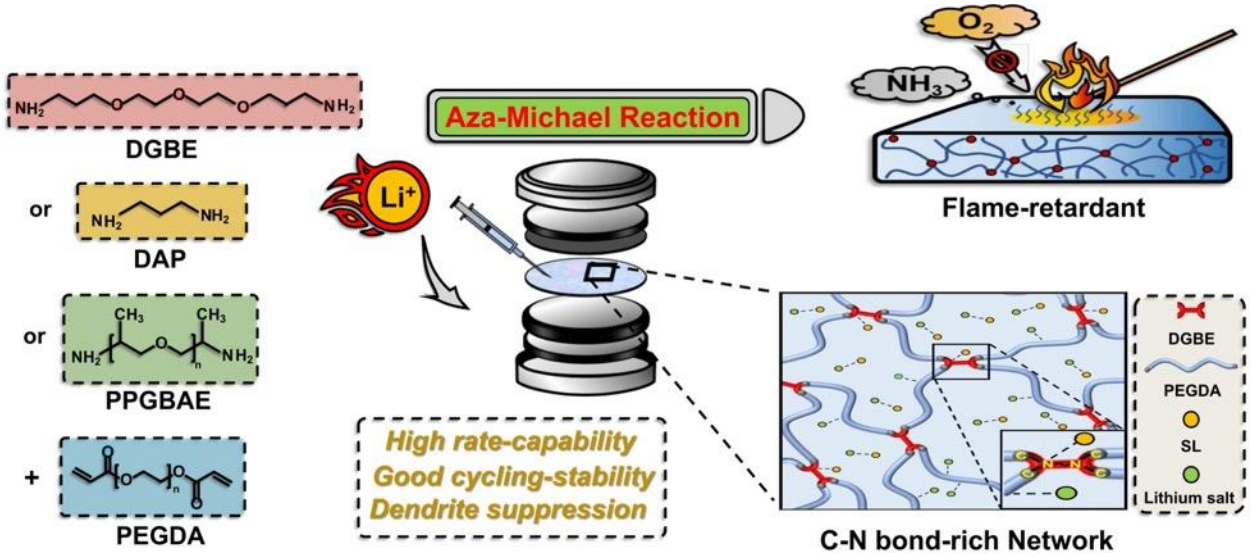

Figure 1. C-N bond-containing non-flammable polymer electrolytes via lithium salt-catalyzed aza-Michael addition.

EXPERIMENTAL SECTION

Materials. Poly(ethylene glycol) diacrylate (PEGDA, M_n = 600, Aladdin), 1,4-butanedioldiacrylate (BDA, 90%, Innochem) and methyl acrylate (MA, 90% , Innochem) were purified by the columns of neutral aluminium oxide (Al_2O_3) to remove residual polymer

inhibitors and then stored in a refrigerator. Propylamine (1-AP, 99%, Aladdin), 1,3-diaminopropane (DAP, 98%, Innochem), diethylene glycol bis(3-aminopropyl) ether (DGBE, 98%, Aladdin), poly(propylene glycol) bis(2-aminopropyl ether) (PPGBAE, M_n = 400, Aladdin), and sulfolane (SL, 98%, Innochem) were used directly without any purification. Before *in-situ* polymerization, above corresponding reagents required three freeze-pump-thaw cycles under argon flow. Bis(trifluoromethane)sulfonimide lithium (LiTFSI, 99%, Aladdin), lithium difluoro(oxalato)borate (LiDFOB, 99.9%, Innochem), lithium perchlorate ($LiClO_4$, 99%, Innochem), lithium hexafluorophosphate ($LiPF_6$, 99%, Innochem) and lithium tetrafluoroborate ($LiBF_4$, 99%, Innochem) were dried in a vacuum oven and then transferred to glovebox for storage. The used cellulose separator (TF4840) has a thickness of 40 μm, a diameter of 16 mm and an areal density of 48 g m^{-2}. The thickness of the *in situ* obtained electrolyte film is around 80 μm to 100 μm. Lithium iron phosphate ($LiFePO_4$), lithium polyacrylate (PAALi, M_n = 450000, Aladdin) and acetylene black (AB) were used for the preparation of anode material.

Simulation Experiment of Lithium Salt-Catalyzed Aza-Michael Addition Reaction. Different lithium salts (0.23 mmol, including $LiClO_4$, LiTFSI, LiDFOB, $LiBF_4$ and $LiPF_6$) were dissolved separately in MA (4.65 mmol), and then mesitylene (1 wt%) was dripped into the solution as a reference reagent. 1-AP (2.32 mmol) was added quickly to the bottle, and the mixed solution was stirred at room temperature. The aliquots were taken from the reaction mixture at different time and then dissolved in $CDCl_3$ for NMR test. The control group is without lithium salt, and other operation are same to the above process. (MA, δ_A = 6.41, 6.12, 5.84 ppm; Momo-Adduct, δ_{B1} = 2.88 ppm, δ_{C1} = 2.58 ppm, δ_{D1} = 2.54 ppm, δ_{E1} = 3.76 ppm, δ_{F1} = 1.52 ppm, δ_{G1} = 0.91 ppm; Bi-Adduct, δ_{B2} = 2.76 ppm, δ_{C2} = 2.45 ppm, δ_{D1} = 2.37 ppm, δ_{E2} = 3.68 ppm, δ_{F2} = 1.43 ppm, δ_{G2} = 0.85 ppm).

$LiClO_4$ was be selected for the qualitative research of linear polymerization by aza-Michael addition. Firstly, $LiClO_4$ (0.05 mmol) and BDA (1 mmol) were uniform mixing, then 1-AP (1 mmol) was dripped into the bottle to proceed the aza-Michael addition. The solution was monitored by ^1H NMR spectrum after 0.6 h, 6 h and 18 h of reaction, respectively. The only difference of control group is that no lithium salt was added, and other operations are same to the above process. The control group did not add $LiClO_4$, but other process was the same. (BDA, δ_a = 6.41, 6.12, 5.84 ppm; Momo-Adduct, δ_{b1} = 1.52 ppm, δ_{c1} = 2.59 ppm, δ_{d1} = 2.53 ppm, δ_{e1} = 2.89 ppm, δ_{f1} = 1.75 ppm, δ_{g1} = 4.19 ppm, δ_{h1} = 0.91 ppm; Linear Polymer, δ_{b2} = 1.42 ppm, δ_{c2} = 2.44 ppm, δ_{d1} = 2.37 ppm, δ_{e2} = 2.77 ppm, δ_{f2} = 1.71 ppm, δ_{g2} = 4.09 ppm, δ_{h1} = 0.85 ppm).

Preparation of Solid Polymer Electrolytes. Preparation of DGBE-PEGDA600 and DAP-PEGDA600: Equimolar DAP or DGBE and PEGDA600 were mixed with LiTFSI:LiDFOB (2:1), and the EO/Li = 20:1, to form a precursor solution. The precursor was then reserved in a vacuum oven at 60 °C for 12 h. Preparation of $PPEGDA_{600}$: PEGDA600 was mixed with LiTFSI:LiDFOB (2:1), and the EO/Li = 20:1, to form a precursor solution. 0.5 wt% AIBN was then added and heated in a vacuum oven at 60 °C for 12 h.

Fabrication of Gel Polymer Electrolytes. LiTFSI (2 mmol), LiDFOB (1 mmol), and SL (15 mmol) were mixed and stirred vigorously at room temperature to form the liquid-state DES. Then, a certain mass of DES was mixed with $PEGDA_{600}$ (1 mmol) and amine monomers (1mmol, including DAP and DGBE) to prepare the reaction precursor. During the battery assembly process, a drop of the precursor liquid was added to the cellulose membrane of the battery. Finally, the battery was assembled *in-situ*, reserved in a vacuum oven at 60 °C for 12 hours to make the reaction complete. Finally, the *in-situ* GPE membrane is named as X-

$PEGDA_{600}$-DES Y (X, the abbreviation of amine monomer; Y, the mass-percentage value of DES relative to overall mass).

Calculation of Crosslinking Density. Dynamic mechanical properties were characterized by the Diamond DMA. Standard samples with diameter of 1cm and thickness of 1 mm were tested in compression mode, while the tested temperature ranges from -80 to 80 °C and the frequency is 1 Hz. The temperature corresponding to the maximum loss modulus was recorded as T_g. The formula for calculating the crosslinking density (ρ) is as follow: $\rho = E'/\phi RT$. Thereinto, E′ is the storage modulus at T_g + 30 °C, ϕ is the front factor which can be approximated to 1 in the Flory theory, R is the gas constant at T_g + 30 °C, and T is the absolute temperature at T_g + 30 °C.

Fabrication of Li/LFP Cells. The $LiFePO_4$ cathode was prepared by casting a slurry of LFP, PAALi, and AB in deionized water on Al foil, and the weight ratio of LFP, PAALi, and AB is 80:10:10. The casted cathode film was dried at 80 °C for 12 h and punched into small plates with a diameter of 16 mm. The mass loading of the active material was ~1.5 mg cm^{-2}. CR2032 coin cells were assembled in the glove box (O_2 < 0.1 ppm; H_2O < 0.1 ppm) under an Ar atmosphere with TF080 as the separator and lithium plates as the anode. The corresponding precursor was injected into the cell, and the cell was then assembled and heated for testing. The cycling performance of the cell was tested at the voltage range from 2.5 V to 4.0 V *vs.* Li/Li^+ on the LAND CT2001A test system (Wuhan Land Electronics Co. Ltd., China) at 60 °C.

Characterization. The thermostability of the solid and gel polymer electrolytes were tested from 30 °C to 800 °C with a heating rate of 10 °C/min through a thermogravimetric analyzer (TGA, PerkinElmer 4000), and the whole process is under a nitrogen (N_2) atmosphere. Their glass transition temperature (T_g) was measured by a differential scanning calorimetry (DSC, Q2000) with a heating rate of 10 °C/min from -90 °C to 100 °C under a N_2 atmosphere.

Electrochemical Performance.

The ionic conductivities (σ) of the polymer electrolytes were evaluated using an electrochemical workstation (Autolab PGSTAT302N, Netherlands), and the tested temperature ranges from 30 to 80 °C. σ can be calculated from the following equation: $\sigma_i = \frac{L}{R_i \times S}$. Thereinto, the film thickness (*D*) and area (*S*) were measured after the end of the EIS measurement, and R_i represents the impedance value at different temperature.

The electrolyte membranes were sandwiched between the lithium and steel sheets to *in-situ* form the batteries, and their electrochemical stability windows were conducted on a test (60°C) of linear sweep voltammetry (LSV) under a potential from 0 to 7 V. The Li|SPE or GPE|Li cell was assembled to reflect the condition of lithium-ion migration under a polarization voltage (ΔV) of 10 mV. The current (I_0), interfacial resistance (R_0) at the outset, and current (I_s), interfacial resistance (R_s) under the stable condition were all recorded to measure the lithium-ion transference number (t_{Li^+}), which can be calculated by equation: $t_{Li^+} = \frac{I_s(\Delta V - I_0 R_0)}{I_0(\Delta V - I_s R_s)}$.

Surface Properties of Lithium Anode.

The lithium symmetric cells assembled with corresponding electrolytes were used for the analysis of interfacial performance after the lithium-deposition cycling (60°C). The surface morphology of the lithium anode was detected by a scanning electron microscopy (SEM, Nova NanoSEM 450). X-ray photoelectron spectroscopy (XPS, AXIS-ULTRA DLD-600W) was applied to analyze the element composition of lithium anodes after the longtime charge-discharge cycling.

RESULTS AND DISCUSSION

Effect of Lithium Salts on the Aza-Michael Addition. In order to ensure a satisfying crosslinked rate for the subsequent construction of polymer electrolytes, the effect of various lithium salts (LiTFSI, $LiClO_4$, LiDFOB, $LiBF_4$ and $LiPF_6$) on the reaction rate was first studied based on monofunctional propylamine (1-AP) and methyl acrylate (MA), in a 1:2 molar ratio, and the detailed calculation process (equation S1 in Supporting Information) and resulting conversion values by ^1H NMR spectra are listed in **Tables S1-S6** (Supporting Information), **Figures S1-S5** (Supporting Information) and **Figure 2a**. In the early stages (< 1 h), the reaction was fast no matter whether salt was present or not, which is consistent with a fast addition of the primary amine to consume one MA equivalent and generate the intermediate secondary amine. The consumption of the second MA equivalent to yield the final tertiary amine product, on the other hand, was much slower, proceeding to less than 10% after 5 h in the absence of lithium salt. A dramatic drop of reactivity on going from a primary to a secondary amine in aza-Michael additions is well established,[45, 46] hence the lithium salts mainly play an accelerated role in the second addition step (**Figure S6**), which can be also confirmed by the quantification of the secondary amine and tertiary amine according to equations S2 and S3. This proposition of lithium salt-catalyzed aza-Michael bis-addition was further clarified by density functional theory (DFT), and the calculation results indicate that the acceleration effect of lithium salts on amine addition not only results from the decrease in activation barrier via the coordination between Li^+ and C=O group, but also contributes to the stabilization of transition state and intermediate. The computational method and results are detailed in the Supporting Information (**Figures S7-S10**).

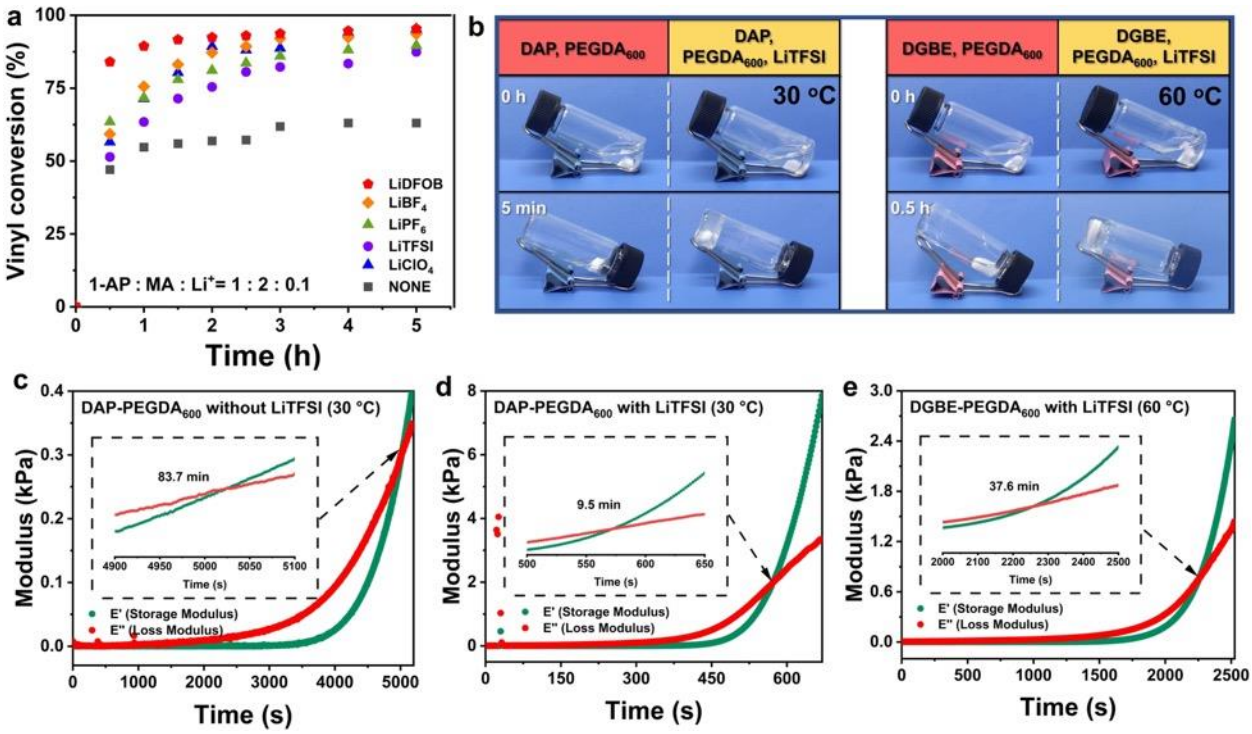

Figure 2. (a) Time evolution of the vinyl conversion for the aza-Michael addition of 1-AP to MA catalyzed by different lithium salts (10%, room temperature). (b) Digital images of the reaction between different diamines and PEGDA accelerated by LiTFSI. (c) Storage and loss modulus of DAP-PEGDA$_{600}$ system without addition of LiTFSI at different time. Storage and loss modulus of DAP-PEGDA$_{600}$ and DGBE-PEGDA$_{600}$ system with addition of LiTFSI at different time.

According to above results, LiTFSI was chosen as the salt, and three different diamines, including 1,3-diaminopropane (DAP), diethylene glycol bis(3-aminopropyl ether) (DGBE) and poly(propylene glycol) bis(2-aminopropyl ether) (PPGBAE) were used to react with PEGDA for preparing crosslinking polymer electrolyte (**Figure 1**). As shown in **Figure 2b** and **Figure S11**, the addition of LiTFSI significantly shortens the solidification time, while the crosslinked rate was also found to depend on the length of the diamine ether due to the decreased concentration of reactive groups in the reaction mixture. For the shortest-chain DAP, the solidification was efficient after only 5 min at room temperature, while the longer the amino chain (DGBE and PPGBAE), the slower the reaction, thus a heating stimulus was needed for the curing process.

The gelation time was quantified by the crossover between the storage and loss modulus, as shown in **Figure 2c-2e**, the gelation times of DAP/PEGDA$_{600}$ systems with and without LiTFSI addition are 83.7 min and 9.5 min at 30 °C, respectively, while longer time about 40 min was observed in DGBE/PEGDA$_{600}$ system under 60 °C heating, which is consistent with above vial experiments. The FT-IR spectra shown in **Figure S12** confirms the complete crosslinking in DGBE/PEGDA$_{600}$ system after 1.5 h heating, and there is almost no residual C=C stretching vibration in the LiTFSI-added system, while a peak is clearly observed for the non-catalyzed one. Most noteworthy is that the obtained crosslinked products are directly usable as lithium-doped solid polymer electrolytes. Therefore, this facile method paves the way to directly obtain polymer electrolytes for LMBs without the need to introduce any non-electrolytic additives.

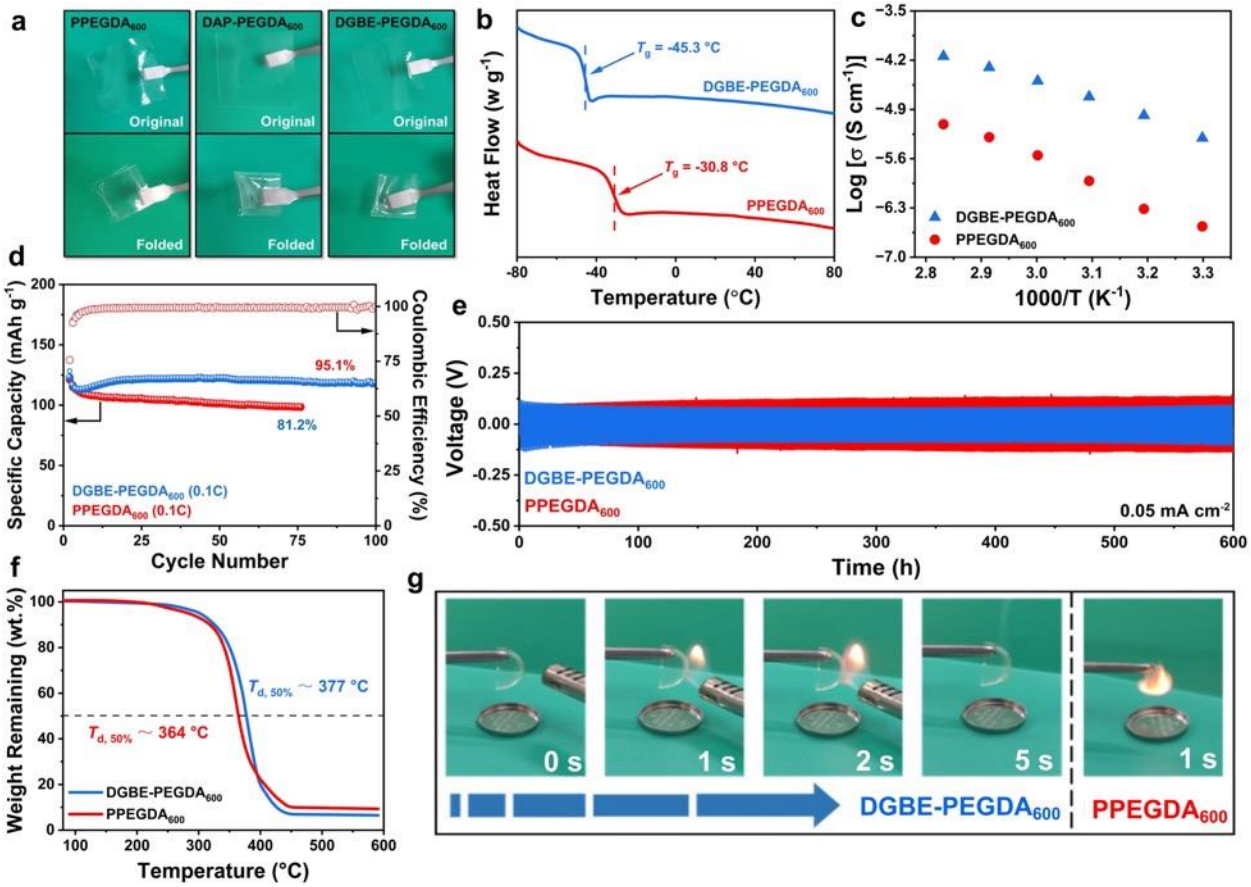

Figure 3. (a) Photographs of $PPEGDA_{600}$, DAP-$PEGDA_{600}$ and DGBE-$PEGDA_{600}$ before and after folding. (b) DSC curves of $PPEGDA_{600}$ and DGBE-$PEGDA_{600}$. (c) Temperature-dependent ionic conductivities of PPEGDA and DGBE-$PEGDA_{600}$. (d) Cycling performance of DGBE-$PEGDA_{600}$ with a rate of 0.1 C at 60 ºC. (e) Voltage profile for plating/stripping experiments in Li symmetric cell cycled at the current density of 0.05 mA cm^{-2} at 60 ºC. (f) TGA curves of PPEGDA and DGBE-$PEGDA_{600}$. (g) Combustion experiments of PPEGDA and DGBE-$PEGDA_{600}$.

Performance Evaluation of Solid PEs Obtained from Aza-Michael Reaction. The physicochemical properties and conducting power of the obtained polymer electrolytes were evaluated to reveal the superiority of the aza-Michael reaction in the structural design and construction of polyether-based LMBs. In comparation, the $PPEGDA_{600}$ was also prepared via conventional AIBN-initiated radical polymerization. As shown in **Figure 3a**, the flexibility of the obtained membranes was examined by a folding test. The $PPEGDA_{600}$ film fractures upon bending, while the crosslinked membranes obtained via the aza-Michael reaction is softer, being freely bent without damage. This feature is due to the lower crosslinking density (ρ) in DAP-$PEGDA_{600}$ and DGBE-$PEGDA_{600}$ membranes relative to $PPEGDA_{600}$ (**Figure S13**), which can be calculated according to the rubber elasticity theory (**Table S8**).[47, 48] In view of the gelation rate for *in-situ* battery preparation and the content of ethyl oxide (EO) group, DGBE-$PPEGDA_{600}$ system was chosen for further study. The inherent crystallinity of the polyether electrolyte is interrupted by the crosslinking structure and the introduction of C-N bonds, thus the adduct of aza-Michael reaction exhibits a lower glass transition temperature (T_g) relative to the C-C crosslinking in $PPEGDA_{600}$, lowering the T_g value to -45.3 ºC (**Figure 3b)**. The increase of the segment mobility is also reflected in the ion conduction (**Figure 3c**) and mechanical properties (**Figure S14**). The ionic conductivity of DGBE-$PPEGDA_{600}$ is higher than that of $PPEGDA_{600}$, and the elongation of DGBE-PEGDA600 (79.9%) is higher than that of PPEGDA600 (33.1%), which is consistent with the above crosslinking density and folding results. In addition, the

insertion of C-N bonds leads to improved redox stability, with a high oxidation voltage of 4.9 V and t_{Li}+ (**Figures S15** and **S16**).

The advantages of the DGBE-PPEGDA$_{600}$ electrolyte also reflect in the *in-situ* prepared lithium metal batteries. As shown in **Figure 3d**, the as-assembled Li/LFP cell can steadily work at 0.1 C (60 ºC) for 100 cycles with a high-capacity retention of 95.1%, while PPEGDA$_{600}$ retains only an 82.1% capacity after 75 cycles under the same operating conditions, indicating that the formed interface between the DGBE-PPEGDA$_{600}$ electrolyte and the electrode is stable. The relatively higher voltage of PPEGDA$_{600}$ in lithium plating-stripping tests carried out for 600 h with a current density of 0.05 mA cm^{-2} also confirms that the C-N inserted polyether is a better Li^+ carrier than the conventional one (**Figure 3e**). More interestingly, the introduction of N atom endows the polyether-based electrolyte with an excellent fire-retardant ability. As shown in **Figure 3f**, the decomposition temperature of DGBE-PPEGDA$_{600}$ with 50% remaining ($T_{d,\,50\%}$) is higher than PPEGDA600, and the PPEGDA$_{600}$ film immediately catches fire, whereas the DGBE-PPEGDA$_{600}$ material cannot be ignited after several seconds (**Figure 3g** and **Movie S1** in Supporting Information). This is because the inserted N atoms generate inert gases (*e.g.* NH_3),[8] which cover the polymer surface, thus restraining the propagation of oxygen radicals. This non-flammability property paves a simple way for the fabrication of high safety polymer electrolytes via structural design.

Performance Optimization via C-N Bonding with Deep Eutectic Solvent. In addition to the flexibility and fire retardancy properties, the structural design with the insertion of C-N bonds also endows the material with the ability to interact with a liquid plasticizer, thus constructing a gel polymer electrolyte for better ion migration. As a common additive in liquid electrolyte, sulfonyl-containing compounds can improve the rate performance of corresponding batteries,

and the interface stability between the electrode and the electrolyte is significantly enhanced via their reductive decomposition. Moreover, the interaction between this compound and lithium salt forms deep eutectic solvent (DES), which can decrease the total viscosity of the precursor and improve the electrode infiltration, which are both beneficial for *in-situ* batteries construction. Hence, sulfolane was chosen to premix with LiTFSI and LiDFOB (SL:LiTFSI:LiDFOB = 5:1:0.5), and the formed DES was used in aza-Michael system for preparing gel polymer electrolyte. LiDFOB is added for further interface-reinforcement due to its easy generation of F- and B-containing solid electrolyte interface.[49] Indeed, gels with improved electrochemical performance could be obtained by adding different content of DES, the obtained gel electrolytes are named PPEGDA-DESx and DGBE-PEGDA$_{600}$-DESx, respectively, where x represents the weight fraction of DES. As shown in **Figure S17**, the introduction of the DES yields a marked increase of the ionic conductivity and of the electrochemical stability window (around 5.5 V), and the ion-migration ability increases with the DES content. Although the observed decomposition temperature of the gel electrolytes is lower than the solid ones, it is sufficiently high to allow battery processing.

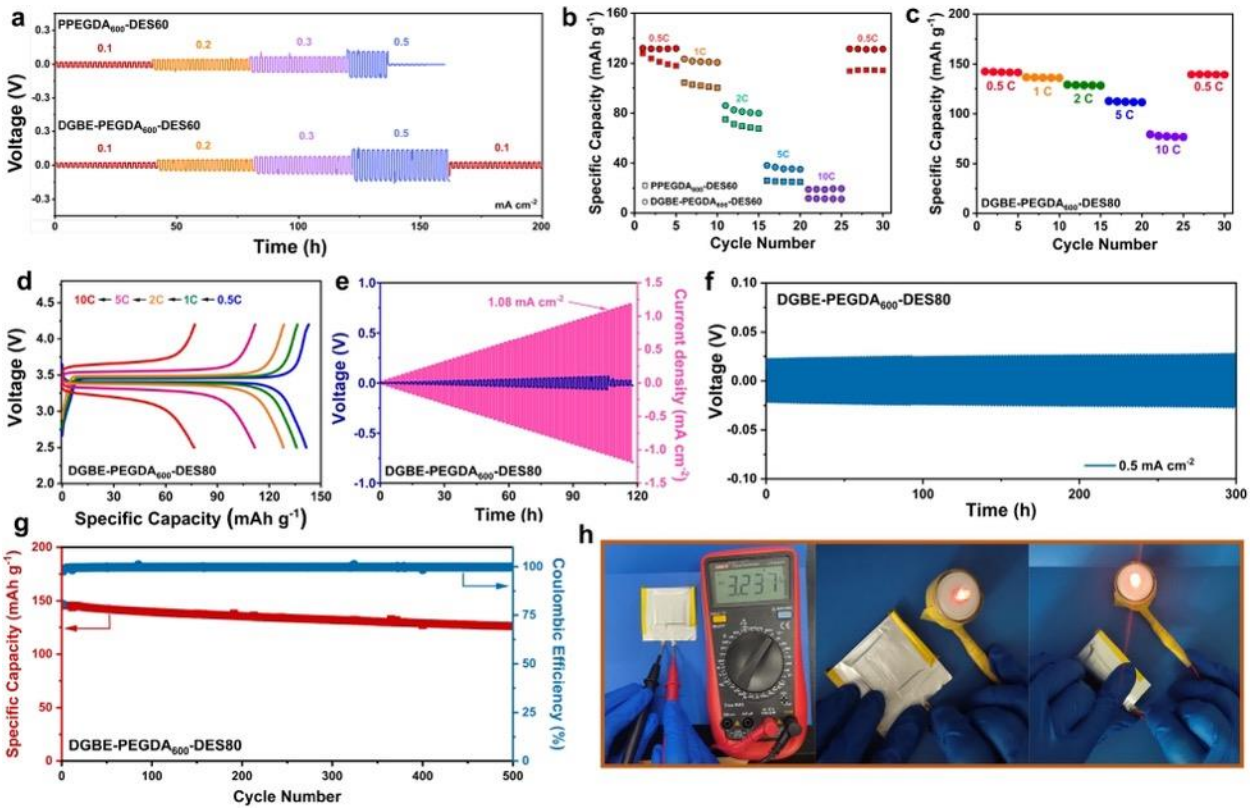

Figure 4. (a) Galvanostatic cycling curves of lithium symmetric cells based on PPEGDA$_{600}$-DES60 and DGBE-PEGDA$_{600}$-DES60 at different current densities. (b) Rate performance of Li|DGBE-PEGDA$_{600}$-DES60|LFP and Li|PPEGDA$_{600}$-DES60|LFP cells. (c) Rate performance of Li|DGBE-PEGDA$_{600}$-DES80|LFP. (d) Charge-discharge curves of Li|DGBE-PEGDA$_{600}$-DES80|LFP cell at different rates. (e) CCD of Li|DGBE-PEGDA$_{600}$-DES80|Li cell. (f) Galvanostatic cycling profiles of the Li|DGBE-PEGDA$_{600}$-DES80|Li symmetrical cell at the current density of 0.5 mA cm^{-2}. (g) Long cycling profiles of the Li|DGBE-PEGDA$_{600}$-DES80|LFP cell at 0.5 C and corresponding charge-discharge curves. All tests were carried out at 60 °C. (h) Photographs of the lamps lightened by the flat and folded Li|DGBE-PEGDA$_{600}$-DES80|LFP pouch cell.

Relative to PPEGDA-DES, the gel electrolyte obtained by the combination of DES and DGBE-PEGDA$_{600}$ matrix exhibits greater advantage. For example, the critical current density (CCD) of the lithium symmetric batteries based on DGBE-PEGDA$_{600}$-DES60 (1.08 mA cm^{-2}) is higher than that of PPEGDA-DES60 (0.75 mA cm^{-2}) (**Figure S18**), and the high crosslinking density Li|PPEGDA-DES60|Li and Li|DES|Li cells short-circuit at the current density of 0.5 and 0.3 mA cm^{-2} (**Figure S18**), respectively, whereas the lithium symmetric cells based on DGBE-

PEGDA$_{600}$-DES60 can steadily work at different current densities, and the more conductive DGBE-PEGDA$_{600}$-DES60 exhibits a lower overpotential (**Figure 4a**). Similar tendency was also observed in the rate performance of Li/LFP batteries, as shown in **Figure 4b**, the Li|DGBE-PEGDA-DES60|LFP cell delivers better cycling stability and higher specific capacities than that in Li|PPEGDA-DES60|LFP cell. Above results are ascribed to the C-N bonds and polar carbonyl groups in DGBE-PEGDA$_{600}$ matrix, which can interact with the SL molecules and with the lithium salts, thus decreasing the drastic reactions and stabilizing the electrode-electrolyte interface.

When DES weight fraction reaches 80 wt%, a high ionic conductivity value of 1.76×10^{-4} S cm^{-1} was obtained at 30 ºC. The charge-discharge process of the resulting Li|DGBE-PEGDA-DES80|LFP cell was significantly enhanced with a slight capacity decay as the current increases. High specific discharge capacities of 112 mAh g^{-1} and 79 mAh g^{-1} were obtained at 5 C and 10 C, respectively (**Figure 4c**). The narrow voltage platform at different rates also reflects the excellent charge-discharge reversibility of the Li|DGBE-PEGDA600-DES80|LFP battery (**Figure 4d**). Further increased current-tolerance is obtained in the Li|DGBE-PEGDA600-DES80|Li cell with the critical current density of 1.08 mA cm^{-2} (**Figure 4e**), and long-term cycling stability is shown under the relatively high current density of 0.5 mA cm^{-2} for 300 h (**Figure 4f**). The Li|DGBE-PEGDA600-DES80|Li battery can also steadily cycle for 600 h (0.1 mA cm^{-2}) without any short-circuit (**Figure S19**). In addition, the full battery assembled with *in-situ* formed DGBE-PEGDA$_{600}$-DES80 has a high initial discharge capacity of 145.2 mAh g^{-1} at 0.5 C and can cycle for 500 cycles with the capacity retention rate of 86.8% (**Figure 4g**), without showing any obvious deteriorating of the voltage platform even after 500 cycles (**Figure S20).** This indicates a good compatibility of this electrolyte with the lithium anode and LFP cathode.

Therefore, the flexibility of the branched DGBE-PEGDA$_{600}$ skeleton permits the assembly of pouch cells for practical application. As shown in **Figure 4h**, the Li|DGBE-PEGDA$_{600}$-DES80|LFP pouch cell was assembled and tested. The initial open-circuit voltage delivered by the cell, after being charged to the upper cutoff voltage of 4.2 V, was 3.24 V. Abuse experiments were then conducted. There was no internal short circuit or failing after a 90^{o} bend, demonstrating a satisfactory flexibility and safety of the DGBE-PEGDA$_{600}$-DES80 electrolyte for advanced lithium metal batteries.

Interfacial Characterization. To gather additional information on the electrolyte-electrode interface of the Li|DGBE-PEGDA$_{600}$-DES80|Li cell, the lithium anode was analyzed by X-ray photoelectron spectroscopy (XPS). For comparison, the lithium symmetric battery assembled with pure DES was also studied. Both cells were cycled for 100 hours at a current density of 0.1 mA cm^{-2}. As shown in **Figures 5a** and **5d**, signals attributable to C-F bonds (C 1s, 293.8 eV; F 1s, 689.0 eV) were clearly observed on the lithium surface of the GPE system, whereas these signals were barely visible for the DES system.[50] Instead, a strong LiF peak (F 1s) appears at 685. 0 eV. This phenomenon indicates that there is extensive reduction of the TFSI^{-} and DFOB^{-} anions in the DES system to generate LiF. The effect of the DGBE-PEGDA$_{600}$ matrix to fix the anions through interacting with the C-N bonds and the polar carbonyl groups inhibits this reduction reaction. Moreover, the introduction of polymer skeleton leads to the formation of ROCO$_2$Li in the solid electrolyte interface (SEI) layer by reacting with the lithium anode, which is suggested by the observation of a peak (O 1s spectrum) (**Figure 5b**). The presence of this organic component in the SEI layer was further supported by the N 1s spectrum. As shown in **Figure 5c**, the N-containing components in the DES system are mainly derived from the decomposition of TFSI^{-} and an extra signal attributable to Li$_x$NO$_y$ (403.12 eV, N 1s) was

detected for the GPE system. In addition, the higher content of Li_2SO_3, LiS and S-S derivatives in the GPE system than that in DES is attributed to the decomposition of the dissociated SL molecules (**Figure 5e**),[51, 52] which are beneficial for stabilizing the electrolyte-electrode interface.[53, 54] In addition, the use of LiDFOB provides a robust B-containing SEI composition (**Figure 5f**).[55] According to the above results, we can clarify that the *in-situ* fabrication of the N-containing crosslinked polymer electrolyte not only decreases the drastic reaction between the active lithium metal and anions, but also provides helpful organic SEI components. The organic-inorganic composite SEI layer of GPE exhibits higher stability than the cell interface assembled with DES, thus providing excellent long-cycle stability and good interfacial compatibility for LMBs.

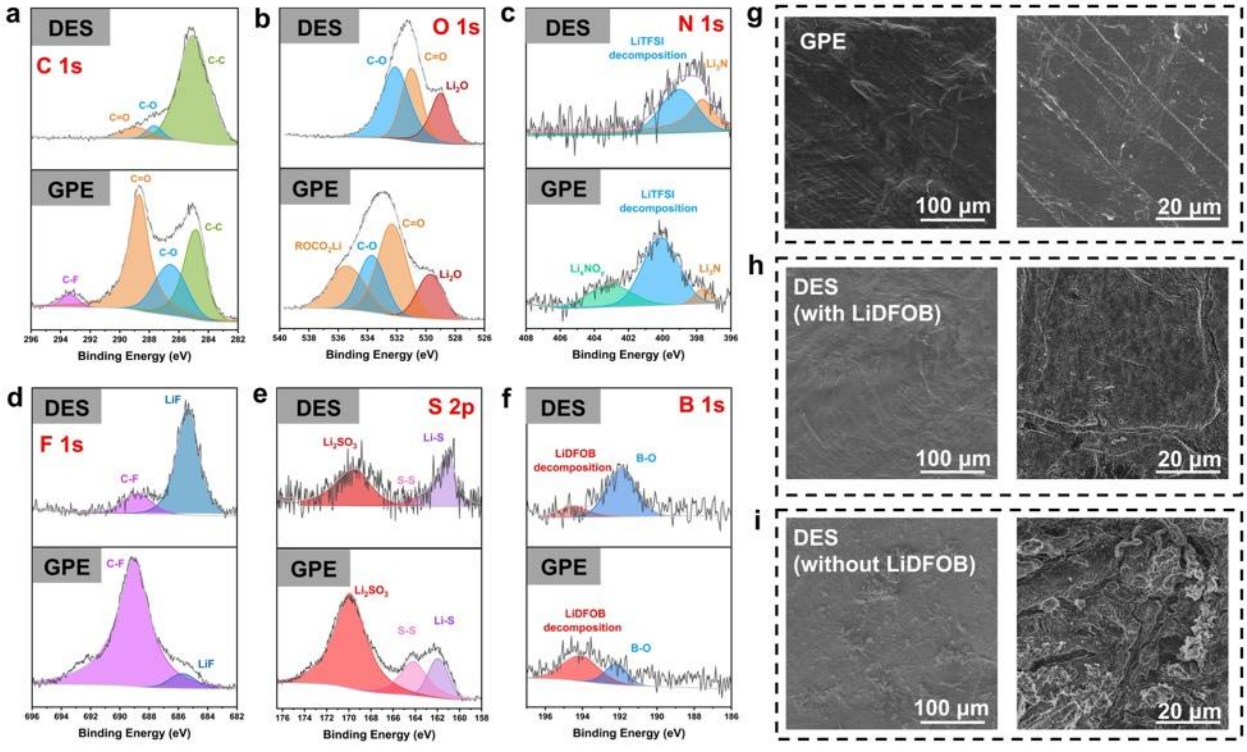

Figure 5. (a) Substance analysis of the SEI layer of the lithium metal anode in the Li|DGBE-$PEGDA_{600}$-DES80|Li cell by (a) C 1s, (b) O 1s, (c) N 1s, (d) F 2p, (e) S 2p and (f) B 1s XPS. SEM images of the micromorphology of lithium metal anodes based on (g) DGBE-$PEGDA_{600}$-DES80, (h) pure DES and (i) DES without LiDFOB under 100 and 20 μm scales. All the lithium anodes were tested after 100 h cycling at the current density of 0.1 mA cm^{-2}.

Scanning electron microscopy (SEM) was then used to explore the anode surface morphology. As shown in **Figures 5g-5i**, after the same time of charging and discharging, the lithium assembled with GPE shows a smooth and flat surface without any evident dendrite growth (**Figure 5g**), while the lithium anode in liquid DES system exhibits tiny cracks and irregularities (**Figure 5h**). These results further confirm the polymer matrix effect on dendrite suppression. When using a DES electrolyte devoid of LiDFOB, evident and uneven protrusions appear on the lithium metal surface (**Figure 5i**), indicating the need of a small amount of LiDFOB in the design of the DES component. The results of both XPS and SEM confirm the positive effect of the C-N bond-containing polymer on the dendrite suppression and cell stability.

CONCLUSIONS

In summary, we have developed a simple and efficient aza-Michael double addition reaction catalyzed by lithium salts. The obtained network structure exhibits relatively low crosslinking density and T_g. Moreover, the insertion of C-N bonds endows the polyether-based polymer electrolyte with additional favorable properties relative to the conventional electrolyte, including excellent flame-retardancy, facile ion transport and better compatibility with a polar SL-containing DES. Hence, a novel and advanced gel polymer electrolyte was prepared by *in-situ* incorporation of the DES into the reaction system. The liquid DES further improves the Li^+ mobility, and its strong interaction with the nitrogen-containing polymer network enhances the interfacial stability. The assembled lithium symmetric battery can withstand a high current density (critical current density of 1.08 mA cm^{-2}) and steadily works for 300 h at the current density of 0.5 mA cm^{-2}. XPS and SEM were used to determine the constitution and morphology of the lithium anode after cycling. In addition, the as-assembled Li/LFP cell could be cycled for

500 cycles at 0.5 C with a capacity retention rate of 86.4%, and the resulting flexible pouch cell was able to lighten up the bulb even after bending. This study provides an extremely promising guide for the structural design of *in-situ* polymer electrolytes and for the preparation of high-performance and safe gel PE systems for LMBs.

ASSOCIATED CONTENT

Supporting Information

^{1}H NMR spectra for conversion calculations (Figures S1-S5 and Tables S1-S6); DFT calculations (Scheme S1; Figures S7-S10 and Table S7); Additional properties of the electrolyte film and corresponding batteries (Figures S11-S20 and Table S8); Movie of ignition test (Movie S1); Additional experimental details, materials, and methods, including photographs of experimental setup.

AUTHOR INFORMATION

Corresponding Authors

Zhigang Xue − *Key Laboratory for Material Chemistry of Energy Conversion and Storage, Ministry of Education, Hubei Key Laboratory of Material Chemistry and Service Failure, School of Chemistry and Chemical Engineering, Huazhong University of Science and Technology, Wuhan 430074, China.*

Email: zgxue@mail.hust.edu.cn

Authors

Jirong Wang − *Key Laboratory for Material Chemistry of Energy Conversion and Storage, Ministry of Education, Hubei Key Laboratory of Material Chemistry and Service Failure, School*

of Chemistry and Chemical Engineering, Huazhong University of Science and Technology, Wuhan 430074, China.

Chi Zhang − *Key Laboratory for Material Chemistry of Energy Conversion and Storage, Ministry of Education, Hubei Key Laboratory of Material Chemistry and Service Failure, School of Chemistry and Chemical Engineering, Huazhong University of Science and Technology, Wuhan 430074, China.*

Yong Zhang − *Key Laboratory for Material Chemistry of Energy Conversion and Storage, Ministry of Education, Hubei Key Laboratory of Material Chemistry and Service Failure, School of Chemistry and Chemical Engineering, Huazhong University of Science and Technology, Wuhan 430074, China.*

Gong Chen − *Key Laboratory for Material Chemistry of Energy Conversion and Storage, Ministry of Education, Hubei Key Laboratory of Material Chemistry and Service Failure, School of Chemistry and Chemical Engineering, Huazhong University of Science and Technology, Wuhan 430074, China.*

Rinaldo Poli − *CNRS, LCC (Laboratoire de Chimie de Coordination), UPS, INPT, Université de Toulouse, 205 route de Narbonne, F-31077 Toulouse, Cedex 4, France*

Xiaolin Xie − *Key Laboratory for Material Chemistry of Energy Conversion and Storage, Ministry of Education, Hubei Key Laboratory of Material Chemistry and Service Failure, School of Chemistry and Chemical Engineering, Huazhong University of Science and Technology, Wuhan 430074, China.*

ORCID

Rinaldo Poli: 0000-0002-5220-2515

Xiaolin Xie: 0000-0001-5097-7416

Zhigang Xue: 0000-0003-2335-9537

Notes

The authors declare no competing financial interest.

ACKNOWLEDGMENT

J.W and C.Z contribute equally. Z.X and J.W are grateful to the National Natural Science Foundation of China (Grant No. 51973073), the Fellowship of China Postdoctoral Science Foundation (2021M701303), and the analytical and testing assistance from the Analysis and Testing Center of HUST for support of this work. R.P is grateful to the CALMIP mesocenter of the University of Toulouse for the allocation of computational resources.

REFERENCES

[1] Chen, S.; Dai, F.; Cai, M. Opportunities and Challenges of High-Energy Lithium Metal Batteries for Electric Vehicle Applications. *ACS Energy Lett.* **2020**, 5, 3140-3151.
[2] Li, S.; Lorandi, F.; Wang, H.; Liu, T.; Whitacre, J. F.; Matyjaszewski, K. Functional Polymers for Lithium Metal Batteries. *Prog. Polym. Sci.* **2021**, 122, 101453.
[3] Wu, F.; Maier, J.; Yu, Y. Guidelines and Trends for Next-generation Rechargeable Lithium and Lithium-ion Batteries. *Chem. Soc. Rev.* **2020**, 49, 1569-1614.
[4] Yoon, K.; Lee, S.; Oh, K.; Kang, K. Challenges and Strategies towards Practically Feasible Solid-State Lithium Metal Batteries. *Adv. Mater.* **2022**, 34, 2104666.
[5] Liu, F. Q.; Wang, W. P.; Yin, Y. X.; Zhang, S. F.; Shi, J. L.; Wang, L.; Zhang, X. D.; Zheng, Y.; Zhou, J. J.; Li, L.; Guo, Y. G. Upgrading Traditional Liquid Electrolyte via In Situ Gelation for Future Lithium Metal Batteries. *Sci. Adv.* **2018**, 4, eaat5383.
[6] Wang, J.; Zhang, C.; Zhang, Y.; Xue, Z. Advances in Host Selection and Interface Regulation of Polymer Electrolytes. *J. Polym. Sci.* **2021**, 60, 743-765.
[7] Wu, F.; Zhang, K.; Liu, Y.; Gao, H.; Bai, Y.; Wang, X.; Wu, C. Polymer Electrolytes and Interfaces toward Solid-State Batteries: Recent Advances and Prospects. *Energy Stor. Mater.* **2020**, 33, 26-54.
[8] Wang, H.; Sheng, L.; Yasin, G.; Wang, L.; Xu, H.; He, X. Reviewing the Current Status and Development of Polymer Electrolytes for Solid-State Lithium Batteries. *Energy Stor. Mater.* **2020**, 33, 188-215.
[9] Chen, G.; Bai, Y.; Gao, Y.; Wang, Z.; Zhang, K.; Ni, Q.; Wu, F.; Xu, H.; Wu, C. Inhibition of Crystallization of Poly(ethylene oxide) by Ionic Liquid: Insight into Plasticizing Mechanism and Application for Solid-State Sodium Ion Batteries. *ACS Appl. Mater. Interfaces* **2019**, 11, 43252-43260.

[10] Zhang, Z.; Ding, J.; Ocko, B. M.; Lhermitte, J.; Strzalka, J.; Choi, C.-H.; Fisher, F. T.; Yager, K. G.; Black, C. T. Nanoconfinement and Salt Synergistically Suppress Crystallization in Polyethylene Oxide. *Macromolecules* **2020**, 53, 1494-1501.
[11] An, Y.; Han, X.; Liu, Y.; Azhar, A.; Na, J.; Nanjundan, A. K.; Wang, S.; Yu, J.; Yamauchi, Y. Progress in Solid Polymer Electrolytes for Lithium-Ion Batteries and Beyond. *Small* **2022**, 18, 2103617.
[12] Mindemark, J.; Lacey, M. J.; Bowden, T.; Brandell, D. Beyond PEO-Alternative Host Materials For Li^+-Conducting Solid Polymer Electrolytes. *Prog. Polym. Sci.* **2018**, 81, 114-143.
[13] Tang, S.; Guo, W.; Fu, Y. Advances in Composite Polymer Electrolytes for Lithium Batteries and Beyond. *Adv. Energy Mater.* **2020**, 11, 2000802.
[14] Verma, P.; Maire, P.; Novák, P. A Review of the Features and Analyses of the Solid Electrolyte Interphase in Li-Ion Batteries. *Electrochim. Acta* **2010**, 55, 6332-6341.
[15] Zhu, T.; Liu, G.; Chen, D.; Chen, J.; Qi, P.; Sun, J.; Gu, X.; Zhang, S. Constructing Flame-Retardant Gel Polymer Electrolytes via Multiscale Free Radical Annihilating Agents for Ni-Rich Lithium Batteries. *Energy Stor. Mater.* **2022**, 50, 495-504.
[16] Long, M.-C.; Wang, T.; Duan, P.-H.; Gao, Y.; Wang, X.-L.; Wu, G.; Wang, Y.-Z. Thermotolerant and Fire-proof Gel Polymer Electrolyte toward High-Performance and Safe Lithium-Ion Battery. *J. Energy Chem.* **2022**, 65, 9-18.
[17] Mi, J.; Ma, J.; Chen, L.; Lai, C.; Yang, K.; Biao, J.; Xia, H.; Song, X.; Lv, W.; Zhong, G.; He, Y.-B. Topology Crafting of Polyvinylidene Difluoride Electrolyte Creates Ultra-Long Cycling High-Voltage Lithium Metal Solid-State Batteries. *Energy Stor. Mater.* **2022**, 48, 375-383.
[18] Meng, N.; Lian, F.; Cui, G. Macromolecular Design of Lithium Conductive Polymer as Electrolyte for Solid-State Lithium Batteries. *Small* **2021**, 17, 2005762.
[19] Wang, J.; Li, S.; Zhao, Q.; Song, C.; Xue, Z. Structure Code for Advanced Polymer Electrolyte in Lithium-Ion Batteries. *Adv. Funct. Mater.* **2021**, 31, 2008208.
[20] Ding, P.; Lin, Z.; Guo, X.; Wu, L.; Wang, Y.; Guo, H.; Li, L.; Yu, H. Polymer Electrolytes and Interfaces in Solid-State Lithium Metal Batteries. *Mater. Today* **2021**, 51, 449-474.
[21] Ma, C.; Cui, W.; Liu, X.; Ding, Y.; Wang, Y. In Situ Preparation of Gel Polymer Electrolyte for Lithium Batteries: Progress And Perspectives. *Infomat* **2021**, 4, 12232.
[22] Wang, Q.; Xu, X.; Hong, B.; Bai, M.; Li, J.; Zhang, Z.; Lai, Y. Molecular Engineering of A Gel Polymer Electrolyte via In-Situ Polymerization for High Performance Lithium Metal Batteries. *Chem. Eng. J.* **2022**, 428, 131331.
[23] Chen, D.; Zhu, M.; Kang, P.; Zhu, T.; Yuan, H.; Lan, J.; Yang, X.; Sui, G. Self-Enhancing Gel Polymer Electrolyte by In Situ Construction for Enabling Safe Lithium Metal Battery. *Adv. Sci.* **2022**, 9, e2103663.
[24] Pei, X.; Li, Y.; Ou, T.; Liang, X.; Yang, Y.; Jia, E.; Tan, Y.; Guo, S. Li-N Interaction Induced Deep Eutectic Gel Polymer Electrolyte for High Performance Lithium-Metal Batteries. *Angew Chem. Int. Ed. Engl.* **2022**, 61, 202205075.
[25] Wang, A.; Geng, S.; Zhao, Z.; Hu, Z.; Luo, J. In Situ Cross-Linked Plastic Crystal Electrolytes for Wide-Temperature and High-Energy-Density Lithium Metal Batteries. *Adv. Funct. Mater.* **2022**, 32, 2201861.
[26] Navarro-Suárez, A. M.; Johansson, P. Perspective-Semi-Solid Electrolytes Based on Deep Eutectic Solvents: Opportunities and Future Directions. *J. Electrochem. Soc.* **2020**, 167, 070511.
[27] Wu, J.; Liang, Q.; Yu, X.; Lü, Q. F.; Ma, L.; Qin, X.; Chen, G.; Li, B. Deep Eutectic Solvents for Boosting Electrochemical Energy Storage and Conversion: A Review and

Perspective. *Adv. Funct. Mater.* **2021**, 31, 2011102.
[28] Wu, H.; Tang, B.; Du, X.; Zhang, J.; Yu, X.; Wang, Y.; Ma, J.; Zhou, Q.; Zhao, J.; Dong, S.; Xu, G.; Zhang, J.; Xu, H.; Cui, G.; Chen, L. Lidfob Initiated In Situ Polymerization of Novel Eutectic Solution Enables Room-Temperature Solid Lithium Metal Batteries. *Adv. Sci.* **2020**, 7, 2003370.
[29] Fu, C.; Ma, Y.; Lou, S.; Cui, C.; Xiang, L.; Zhao, W.; Zuo, P.; Wang, J.; Gao, Y.; Yin, G. A Dual-Salt Coupled Fluoroethylene Carbonate Succinonitrile-Based Electrolyte Enables Li-Metal Batteries. *J. Mater. Chem. A* **2020**, 8, 2066-2073.
[30] Ogawa, H.; Mori, H. Lithium Salt/Amide-Based Deep Eutectic Electrolytes for Lithium-Ion Batteries: Electrochemical, Thermal And Computational Study. *Phys. Chem. Chem. Phys.* **2020**, 22, 8853-8863.
[31] Hwang, S. S.; Cho, C. G.; Kim, H. Room Temperature Cross-Linkable Gel Polymer Electrolytes for Lithium Ion Batteries by In Situ Cationic Polymerization of Divinyl Ether. *Electrochem. Commun.* **2010**, 12, 916-919.
[32] Lu, Q.; He, Y. B.; Yu, Q.; Li, B.; Kaneti, Y. V.; Yao, Y.; Kang, F.; Yang, Q. H. Dendrite-Free, High-Rate, Long-Life Lithium Metal Batteries with a 3D Cross-Linked Network Polymer Electrolyte. *Adv. Mater.* **2017**, 29, 1604460.
[33] Wei, J.; Yue, H.; Shi, Z.; Li, Z.; Li, X.; Yin, Y.; Yang, S. In Situ Gel Polymer Electrolyte with Inhibited Lithium Dendrite Growth and Enhanced Interfacial Stability for Lithium-Metal Batteries. *ACS Appl. Mater. Interfaces* **2021**, 13, 32486-32494.
[34] Mather, B. D.; Viswanathan, K.; Miller, K. M.; Long, T. E. Michael Addition Reactions in Macromolecular Design for Emerging Technologies. *Prog. Polym. Sci.* **2006**, 31, 487-531.
[35] Rulev, A. Y. Aza-Michael Reaction: Achievements and Prospects. *Russ. Chem. Rev.* **2011**, 80, 197-218.
[36] Akinc, A.; Lynn, D. M.; Anderson, D. G.; Langer, R. Parallel Synthesis and Biophysical Characterization of A Degradable Polymer Library For Gene Delivery. *J. Am. Chem. Soc.* **2003**, 125, 5316-5323.
[37] Peyrton, J.; Avérous, L. Aza-Michael Reaction as A Greener, Safer, and More Sustainable Approach to Biobased Polyurethane Thermosets. *ACS Sustain. Chem. Eng.* **2021**, 9, 4872-4884.
[38] Zhou, H.; Xiang, X.; Ma, B.; Wang, G.; Zhang, Z.; Yang, J. Lithium Chloride Catalyzed Aza-Michael Addition of Pyrazoles to α,β-Unsaturated Imides. *Synthesis* **2019**, 51, 3142-3150.
[39] Just, D.; Hernandez-Guerra, D.; Kritsch, S.; Pohl, R.; Císařová, I.; Jones, P. G.; Mackman, R.; Bahador, G.; Jahn, U. Lithium Chloride Catalyzed Asymmetric Domino Aza-Michael Addition/[3 + 2] Cycloaddition Reactions for the Synthesis of Spiro- and Bicyclic α,β,γ-Triamino Acid Derivatives. *Eur. J. Org. Chem.* **2018**, 2018, 5213-5221.
[40] Azizi, N.; Saidi, M. R. $LiClo_4$ Accelerated Michael addition of Amines to A,B-Unsaturated Olefins Under Solvent-Free Conditions. *Tetrahedron Lett.* **2004**, 60, 383-387.
[41] Naga, N.; Inose, D.; Ishida, T.; Kubota, K.; Nageh, H.; Nakano, T. Synthesis of Polymer Networks by Means of Addition Reactions of Tri-Amine and Poly(Ethylene Glycol) Diacrylate or Diglycidyl Ether Compounds. *Polym. Bull.* **2020**, 78, 2745-2763.
[42] Gao, X.; Jin, Z.; Tan, X.; Zhang, C.; Zou, C.; Zhang, W.; Ding, J.; Das, B. C.; Severinov, K.; Hitzeroth, II; Debata, P. R.; He, D.; Ma, X.; Tian, X.; Gao, Q.; Wu, J.; Tian, R.; Cui, Z.; Fan, W.; Huang, Z.; Cao, C.; Bao, Y.; Tan, S.; Hu, Z. Hyperbranched Poly(Beta-Amino Ester) Based Polyplex Nanopaticles for Delivery of CRISPR/Cas9 System and Treatment of HPV Infection Associated Cervical Cancer. *J. Control. Release* **2020**, 321, 654-668.
[43] Liu, Y.; Li, Y.; Keskin, D.; Shi, L. Poly(beta-Amino Esters): Synthesis, Formulations, and

Their Biomedical Applications. *Adv. Healthc Mater.* **2019**, 8, 1801359.
[44] Feng, J.; Xu, X.; Xu, Z.; Xie, H.; Song, P.; Li, L.; Huang, G.; Wang, H. One-Pot, Solvent- and Catalyst-Free Synthesis of Polyphosphoramide as An Eco-Benign and Effective Flame Retardant for Poly(lactic acid). *ACS Sustain. Chem. Eng.* **2020**, 8, 16612-16623.
[45] Wu, D. C.; Liu, Y.; He, C. B.; Chung, T. S.; Goh, S. T. Effects of Chemistries Of Trifunctional Amines On Mechanisms Of Michael Addition Polymerizations With Diacrylates. *Macromolecules* **2004**, 37, 6763-6770.
[46] Cheng, W.; Wu, D.; Liu, Y. Michael Addition Polymerization of Trifunctional Amine and Acrylic Monomer: A Versatile Platform for Development of Biomaterials. *Biomacromolecules* **2016**, 17, 3115-3126.
[47] Zhao, S.; Abu-Omar, M. M. Renewable Epoxy Networks Derived from Lignin-Based Monomers: Effect of Cross-Linking Density. *ACS Sustain. Chem. Eng.* **2016**, 4, 6082-6089.
[48] Nouailhas, H.; Aouf, C.; Le Guerneve, C.; Caillol, S.; Boutevin, B.; Fulcrand, H. Synthesis and Properties of Biobased Epoxy Resins. Part 1. Glycidylation of Flavonoids by Epichlorohydrin. *J. Polym. Sci., Part A: Polym. Chem.* **2011**, 49, 2261-2270.
[49] Huang, S.; Wang, S.; Hu, G.; Cheong, L.-Z.; Shen, C. Modulation of Solid Electrolyte Interphase of Lithium-Ion Batteries by lidfob and libob Electrolyte Additives. *Appl. Surf. Sci.* **2018**, 441, 265-271.
[50] Fu, J.; Ji, X.; Chen, J.; Chen, L.; Fan, X.; Mu, D.; Wang, C. Lithium Nitrate Regulated Sulfone Electrolytes for Lithium Metal Batteries. *Angew Chem. Int. Ed. Engl.* **2020**, 59, 22194-22201.
[51] Yao, W.; Zhang, Z.; Gao, J.; Li, J.; Xu, J.; Wang, Z.; Yang, Y. Vinyl Ethylene Sulfite as A New Additive in Propylene Carbonate-Based Electrolyte for Lithium Ion Batteries. *Energy Environ. Sci.* **2009**, 2, 1102-1108.
[52] Parimalam, B. S.; Lucht, B. L. Reduction Reactions of Electrolyte Salts for Lithium Ion Batteries: $lipf_6$, $libf_4$, lidfob, libob, and litfsi. *J. Electrochem. Soc.* **2018**, 165, A251-A255.
[53] Xu, C.; Sun, B.; Gustafsson, T.; Edström, K.; Brandell, D.; Hahlin, M. Interface Layer Formation in Solid Polymer Electrolyte Lithium Batteries: An XPS Study. *J. Mater. Chem. A* **2014**, 2, 7256-7264.
[54] Li, S.; Xu, X.; Shi, X.; Li, B.; Zhao, Y.; Zhang, H.; Li, Y.; Zhao, W.; Cui, X.; Mao, L. Composition Analysis of the Solid Electrolyte Interphase Film on Carbon Electrode of Lithium-Ion Battery Based on Lithium Difluoro(Oxalate)Borate and Sulfolane. *J. Power Sources* **2012**, 217, 503-508.
[55] Xu, M.; Zhou, L.; Hao, L.; Xing, L.; Li, W.; Lucht, B. L. Investigation and Application of Lithium Difluoro(oxalate)borate (LiDFOB) as Additive to Improve the Thermal Stability of Electrolyte for Lithium-Ion Batteries. *J. Power Sources* **2011**, 196, 6794-6801.